Sensors & Actuators: B. Chemical 336 (2021) 129727

Contents lists available at ScienceDirect

Sensors and Actuators: B. Chemical

journal homepage: www.elsevier.com/locate/snb

Inkjet-printed flexible silver electrodes on thiol-enes

Eero Kuusisto [a,1], Joonas J. Heikkinen [a,1], Päivi Järvinen [b], Tiina Sikanen [b], Sami Franssila [a], Ville Jokinen [a,*]

[a] Department of Chemistry and Materials Science, School of Chemical Engineering, Aalto University, Tietotie 3, Micronova, 02150, Espoo, Finland
[b] Drug Research Program, Division of Pharmaceutical Chemistry and Technology, Faculty of Pharmacy, University of Helsinki, Finland

ARTICLE INFO

Keywords:
Stretchable electronics
Metallization
Electrochemical impedance spectroscopy
BioMEMS
Off-stoichiometric thiol-enes

ABSTRACT

Flexible and conductive silver electrodes were fabricated by inkjet printing on several different compositions of thiol-ene polymers. Conductive electrodes with resistivity down to 30 μΩcm and good adhesion of the electrodes were obtained by optimizing the printing parameters. The maximum printing resolution was 100 μm lines and 80 μm gaps between the lines. Printing on top of cross-linked off-stoichiometric thiol-ene polymer was tested for compositions ranging from 30 % thiol excess to 5 % allyl ('ene') excess. The roughness off the thiol-ene surfaces was shown to greatly improve the quality of the printed electodes: consistently high yield of conductive electrodes was obtained on rough surfaces (roughness ≈ 1 μm), whereas on smooth surfaces the electrodes were often cracked. The lowest resistivity values were obtained on electrodes printed on near stoichiometric thiol-ene substrates. The conductivity of the electrodes was retained after 5 % linear strain and after repeated bending with 1 mm radius of curvature, showing the potential for flexible sensors. The electrodes were also applied to electrical impedance-based monitoring of cell growth on thiol-ene surfaces, which showcased that the electrodes survive stressed cell culture conditions for at least 36 h.

1. Introduction

Inkjet printing technology enables direct deposition of functional materials on different substrates. It has been used for fabricating a range of flexible and wearable electronic devices [1] and biochips [2]. Examples of inkjet-printed devices include all-polymer transistors [3], polymer solar cells [4], glucose sensors [5] and artificial biological tissues [6]. The materials that can be inkjet-printed include polymers [3], metals [5,7,8], graphene [9], carbon nanotubes [10], biomolecules [11] and cells [6]. In BioMEMS applications, inkjet printing is used to fabricate e.g., solders [12], transistors [13] and electrodes [7]. The use of printed electronics has grown drastically since nanoparticle-based metal inks were introduced [14,15]. These allow conductive metal patterns to be deposited on practically any planar substrate. Polymer substrates are usually preferred in flexible electronics, as they are often durable and can be made transparent. Thermoplastics, such as polyethylene terephthalate (PET) and polycarbonate (PC), are common polymer substrates used in inkjet printing [14,16]. However, inkjet printing on polymer substrate tends to lead challenges in adhesion due to the generally low surface energies of polymers. To overcome adhesion issues, the printed patterns can be laminated in between two films which encapsulate the metal pattern [13,17]. Adhesion can also be improved by roughening the polymer surface [18], although increasing surface roughness has also been reported to increase the resistivity of the printed metal [19]. Polydimethylsiloxane (PDMS) elastomer is the most used material for microfluidics due to its straightforward processability by molding, good optical transparency, high oxygen permeability and lack of toxicity [20,21]. The relatively high hydrophobicity combined with the relatively non-reactive methyl surface chemistry of PDMS however brings a significant challenge for inkjet printing as the elastomer surface does not support uniform wetting or adhesion of the metal nanoparticles [22,23]. Surface topography modifications can improve adhesion [24,25], but ink delamination by physical agitation remains a problem for most polymer-based printing media.

Thiol-enes are thermoplastic elastomers composed of thiol and allyl monomers crosslinked by ultraviolet (UV)-initiated click chemistry [26] enabling their microfabrication either via direct photolithography or replica molding. Changing the monomer ratio allows tailoring the mechanical properties of thiol-enes from rigid to elastic [27–29]. The resulting thiol-ene polymers are usually transparent, chemically inert

* Corresponding author.
E-mail address: ville.p.jokinen@aalto.fi (V. Jokinen).
[1] Equal Contribution.

https://doi.org/10.1016/j.snb.2021.129727
Received 1 December 2020; Received in revised form 26 February 2021; Accepted 1 March 2021
Available online 3 March 2021

(toward solvents) and sometimes, depending on the composition, cell-compatible [27,30]. A clear advantage of thiol-enes is their tunable surface chemistry that can be tailored to yield free thiol or allyl ('ene') functional groups on the surface [28,31,32] for further functionalization reactions. These surface chemistries can also bond with ink-jet printed materials, for example, thiol groups are known to bond to metals, especially gold [33].

Here, direct inkjet printing of silver electrodes on top of thiol-enes is demonstrated. The process enables conductive electrodes down to 100 μm width and the gaps down to 80 μm to be printed. Rough thiol-ene substrates are used to increase the adhesion and integrity of the metal wires. The durability of the printed electrodes in moist, stressed conditions (37 °C, for 36 h) was tested by culturing adherent Balb 3T3 fibroblasts on the electrodes and monitoring the cell monolayer integrity based on electrical impedance spectroscopy to ensure that e.g., leaching monomers or ink-derived contaminants did not deteriorate the cell viabiliy.

2. Materials and methods

2.1. Thiol-ene fabrication

The chemicals used for thiol-ene fabrication were trimethylolpropane diallyl ether (TMPDE), trimethylolpropane tris(3-mercaptopropionate) (TMPTMP), and Diphenyl(2,4,6-trimethylbenzoyl)phosphine oxide (TPO) (all from Sigma Aldrich). TPO acted as a photoinitiator to initiate the click-reaction to polymerize the thiol-ene. The masses (g) of TMPDE and TMPTMP were calculated with Eq. 1, where e is the thiol excess percentage, and t and a are the numbers of functional groups per monomer; $t = 3$ for trithiol and $a = 2$ for diallyl. The mass (g) of TPO was 0.5 wt-% from the total mass.

$$m_{\text{thiol}} = m_{\text{total}} \Big/ \left(1 + \frac{t/a}{1+e}\frac{M_{\text{allyl}}}{M_{\text{thiol}}}\right) \quad (1)$$

First, TMPDE and TPO were mixed in a beaker, stirred, and heated in a 70 °C oven for 5 min to dissolve the TPO powder. After the solution cooled down, TMPTMP was added, and the solution was stirred for ca. 1 min until it was clear. After stirring, the solution was kept in the oven at 70 °C for another 5 min. To fabricate a rough thiol-ene substrate, a single side polished 100 mm silicon wafer was placed in a Petri dish so that the unpolished side was facing up, and the monomer mixture was poured on top of the silicon wafer and cured under UV flood exposure lamp (ECE 2000, 400 W, λ = 365 nm, Dymax) for 60 s. The crosslinked thiol-ene substrate was carefully detached from the silicon wafer after several minutes of cooling down after UV treatment. To fabricate a smooth thiol-ene surface, the same process was used except the thiol-ene solution was poured on onto an empty Petri dish and the top surface (in contact with air during curing) was used as the smooth surface. In addition to surface roughness, the impact of bulk composition on the quality of metallization was examined using 5 % allyl (functional group) excess, stoichiometric ratio, and 5 %, 7 %, 10 %, or 30 % thiol (functional group) excess in the monomer mixture.

2.2. Printing parameters

The silver electrodes were printed on rough and smooth thiol-ene surfaces using inkjet material printer (Dimatix Materials Printer DMP-2831, Fujifilm) and silver nanoparticle ink (DGP 40LT-15C from Advanced Nano Products). The ink contained 30–35 wt-% of silver nanoparticles in triethylene glycol monoethyl ether solvent and its viscosity and surface tension are 10–17 cP s and 35–38 mN/m respectively. The printer had 16 piezoelectric nozzles, from which 2 or 3 adjacent nozzles were selected for each print. The firing voltage for each nozzle was tuned individually and set to 21 ± 1 V to get the droplets to fall identically from each nozzle. The jetting frequency was kept constant at 20 kHz. The printer platen was held at 60 °C to improve the evaporation of the solvent. Two droplet spacings were tested: 15 μm and 30 μm. The electrode designs were drawn with the printer's built-in software. For all samples, a single layer of ink was printed. The electrode's direction was selected to preferably be the same as the movement of the printer head, making the electrodes more consistent than if printed lengthwise. After the ink had dried on the printer platen, the samples were sintered in an IR-oven (Infrared IC heater T-962, Puhui) at 125 °C for 7 min. The samples were sintered after the ink was completely dry, because wet sample sintering led to bubbles on top of the sample without any adhesion to the thiol-ene (Fig. S1).

2.3. Electrode and substrate characterizations

Resistance of the printed silver electrodes (at least 2 separate electrodes on a sample and at least 2 separate samples of each type measured) was measured with 2-point multimeter (MAS830 L, Mastech). A stylus profilometer (Dektak XT, Bruker) was used to measure the roughness of the electrodes. The roughness was measured using 600 μm long scan. The reported roughness values are the average ± the standard deviation (one sample of each type, 3 measurements per sample) for the rms roughness Pq. The thickness of the electrodes on top of a smooth substrate and electode cracking was measured by scanning electron microscopy (SEM) (Supra 40, Zeiss). Two separate samples with 10 measurements from each sample were measured and reported as the average ± the standard deviation. Optical microscope (Optiphot-2, Nikon) with top and bottom lightning (Halogen 12 V 100 W, Nikon) and a microscope camera (KY-F55B 3−CCD color video camera, JVC) was used to analyze the spreading of the ink, pinhole quantity and vulnerability to cracking. The widths of the electrodes were measured by optical microscope. The reported values are averages and standard deviations obtained from a total of 25 data points for each composition (5 different images of the electrode and measurement from 5 places from each image). Static contact angles of the ink on rough thiol-enes with different compositions were measured with optical goniometry (Theta, Biolin Scientific) using 6 μL droplets. The reported values are the average ± the standard deviation (n = 3). The stretching experiments were carried out with an in-house built machine. The bending experiments were performed manually.

2.4. EIS chip fabrication

The thiol-ene used for electrochemical impedance spectroscopy was fabricated with stoichiometric recipe ($e = 0$ in Eq. 1). For printing, droplet spacing of 30 μm, and thiol-ene thickness of 2 mm were used. Glass chambers (diameter 3 cm) were glued on top of the print on the EIS chips to make suitable wells for the cells to grow and to keep the contact pads out of the cell-growing. The gluing was achieved by dipping the glass chamber slightly in the monomer mixture with the same composition as the chip itself, then placed on top of the print, and cured in UV-oven for 2 × 30 s to minimize the amount of leaking monomers and to ensure the bond holds.

2.5. Electrochemical impedance spectroscopy

Prior to use, the thiol-ene wells incorporating the EIS electrodes were sterilizedwith 70 % (v/v) ethanol (aq). Next, the surfaces were coated with 1% (v/v) Geltrex (Gibco, Thermo Fisher Scientific) in serum free DMEM medium for 1 h (37 °C). Balb 3T3 mouse embryonic fibroblasts (clone A31, European Collection of Authenticated Cell Cultures 86,110,401) were plated into the wells (500 000 cells/well) in complete medium consisting of Dulbecco's Modified Eagle's Medium (high glucose DMEM ready mix, 4.5 g/L glucose, Sigma Aldrich) supplemented with 5-% Fetal Bovines Serum (FBS, Gibco), 5% New Born Calf's Serum (NBCS, Gibco), and 1% (v/v) Pen/Strep (10 000 units/mL penicillin and 10 000 μg/mL streptomycin, Gibco).

The cell impedance spectra were recorded once every hour for 36 h with PalmSens4 potentiostat (PalmSens BV) using 44 data points between 5–100 000 Hz, and compared with cell-free control (at 0 h) using optimum frequency that provided the highest signal.

After culturing, the live and dead cells and all cell nulei were stained using Calcein AM (1 μM, Invitrogen), propidium iodide (2 drops/mL, ReadyProbes Reagent, Invitrogen), and Hoechst 33,342 (2 drops/mL, NucBlue Live ReadyProbes Reagent, Invitrogen), respectively. The cells were imaged using inverted epifluorescence microscope (AxioVert A1 FL, Carl Zeiss Oy) equipped with a broadband lamp (Illuminator HXP 120 V, Leistungselektronik JENA GmbH) and a color CCD camera (Axiocam 305, Zeiss), or an upright epifluorescence microscope (AxioScope A1, Zeiss) equipped with halogen broadband lamp (HAL 100, Zeiss) and the color CCD camera.

3. Results and discussion

3.1. Description of the developed printing process

The fabrication scheme for printed metal patterns on thiol-ene is shown in Fig. 1. The main steps of the fabrication process are: i) producing a smooth or rough thiol-ene substrate by UV click polymerization. The smooth thiol-ene was obtained from the top side of thiol-ene cast on an empty Petri dish. The rough thiol-ene was obtained by replica molding from the unpolished backside of a silicon wafer (Fig. 1a), ii) inkjet printing of Ag-nanoparticle ink on thiol-ene (Fig. 1b), and iii) sintering the ink in infrared (IR)-oven (Fig. 1c). On the basis of preliminary characterization, the rough substrate was shown to provide better ink adhesion and metal integrity than that achieved on the smooth substrate. Electrodes printed on top of the smooth substrates had cracks and were not conductive (Fig. 2a). Therefore, all further experiments were performed utilizing rough thiol-ene surfaces as substrates, which resulted in good metal integrity and conductivity (Fig. 2b and c). Characterization of the topography revealed that the rough surface consists of rectangular truncated pyramids (Fig. 2b) with tens of μm lateral dimensions and overall RMS roughness of ≈ 1 μm (Table 1).

The silver ink was deposited using inkjet material printer (DMP-2831, Fujifilm). The average diameter of droplets printed on the rough thiol-ene substrate was 75 μm. The droplet center-to-center spacing was varied between 15 μm and 30 μm and was found to significantly affect the printing quality. The 30-μm spacing ensured adequate overlap of adjacent droplets to yield continuous electrodes. The droplets dried evenly and quickly, and the samples could be sintered within a minute after printing. The 15-μm spacing resulted in greater overlap of the droplets and therefore more ink was deposited compared to the 30-μm spacing. However, this led to more uneven and slower drying, and lower yield of the electrodes due to increased cracking. This was especially an issue with the contact pads, where a lot of ink was deposited, and the uneven resulted in poor ink adhesion (Fig. S1). However, the resistances achieved with 15-μm spacing were ca. four times lower than with 30-μm spacing because of the greater amount of deposited silver per unit area. Therefore, 15-μm drop spacing was used for characterizing the conductivity of the electrodes, and 30-μm drop spacing for all other experiments, including the electrochemical impedance spectroscopy (EIS) chip.

In this study, the silver ink was sintered in an IR oven and the sintering temperature was set to 125 °C. The ink used in this study requires at least 120 °C sintering temperature, whereas at temperatures above 130 °C, thiol-enes suffer from significant deformation and bending due to thermal expansion. The coefficients of thermal expansion of thiol-enes have been reported to range from 128 $*10^{-6}$ K^{-1} to 151$*10^{-6}$ K^{-1} [34], compared with 300 $*10^{-6}$ K^{-1} for PDMS [35].

3.2. Effect of thiol-ene composition on the printing quality

Changing the ratio of thiol and allyl monomers in bulk polymer composition has an effect on thiol-ene surface chemistry, which affects both the surface properties, such as wettability, and the bulk properties, such as glass transition temperature. These differences in surface and bulk properties may further affect the metal adhesion and overall quality of the printed electrodes. To examine these impacts, several different bulk compositions of thiol-enes were studied as the substrate, ranging from 30 % molar excess of thiol functional groups to 5 % molar excess of allyl functional groups. Based on visual characterization, none of the electrodes had visible cracks. The resistances were measured with electrodes that were 36 mm long and nominally 0.3 mm wide. The resistances are given in Table 1. There was some variation between separate prints and the range given covers the values obtained for each type of substrate. For example, the sample with the overall lowest resistances measured was a 5% thiol excess sample with average resistance of 9.5 Ω ± 3.2 Ω (n = 5) whereas a repeat sample with the same parameters had resistances of 22.7 Ω ± 8.3 Ω (n = 7). The first clear conclusion is that there was a huge degradation in the conductivity when the thiol excess was 7% or higher compared to the compositions closer to stoichiometric and kΩ and MΩ resistances were obtained for those compositions. The samples with the most conductive electrodes were the stoichiometric and the 5% thiol excess and our data is unable to distinguish between these two. The final sample, with 5% allyl excess, had resistances about 2–5 times higher than the stoichiometric and the 5% thiol excess samples while remaining much more conductive than the 7% or higher thiol excess samples.

To estimate the resistivity and conductivity, the nominal width of the electrodes and the thickness measured from an electrode printed on the smooth substrate were used. This is due to the difficulties in measuring the exact thickness of the silver layer on top of rough substrates. However, since the amount of ink that is printed per unit length remains constant, the cross-sectional area of the electrode remains roughly the same. The thicknesses of these electrodes on smooth samples were measured to be ca. 3.8 μm ± 1.1 μm. For the most conductive sample (5% thiol excess substrate with average resistance 9.5 Ω over 5 separate electrodes), these values lead to an estimate for the resistivity of ca. 30 μΩcm (corresponding conductivity of ca. $3*10^6$ S/m). This matches closely with the minimum resistivity of 11.5 μΩcm (conductivity $8.7*10^6$ S/m) reported by the manufacturer of the silver ink and is ca. 20 times higher compared to bulk silver. The resistivity is similar to that reported for printed silver on polymers; for example, Wu et al. [36] reported a resistivity of 27 μΩcm for printed silver electrodes on Kapton and Chung et al. reported a resistivity of ca. 70 μΩcm for printed silver electrodes on PDMS [24].

To investigate the mechanisms behind the conductivity differences,

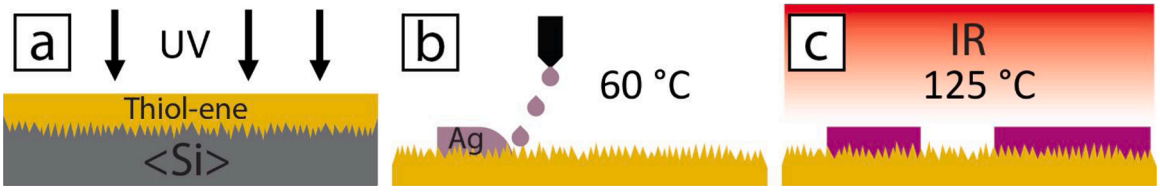

Fig. 1. Inkjet-printed silver lines on thiol-ene substrate (a) Schematic fabrication of rough thiol-ene substrate. (b) Direct inkjet printing of silver nanoparticle ink on rough thiol-ene substrate. (c) Sintering of the nanoparticles with infrared (IR).

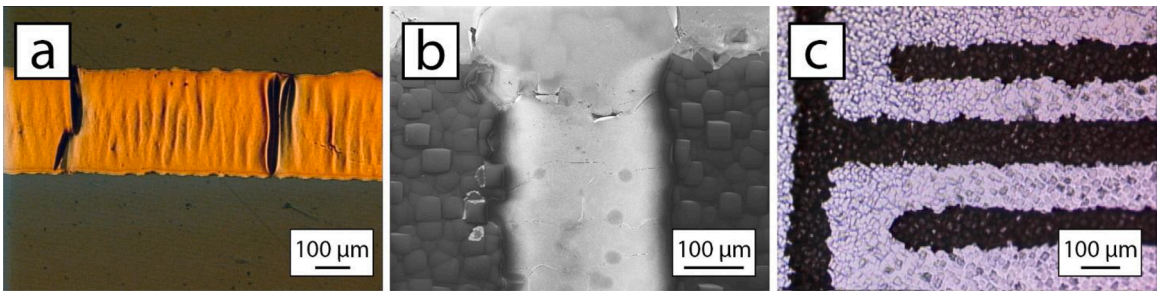

Fig. 2. Images of inkjet-printed silver lines. (a) Microscope image of an electrode printed on smooth thiol-ene substrate shows Ag is prone to cracks (black lines). (b) SEM image of printed electrode with 15-µm droplet spacing on a rough thiol-ene substrate. (c) The smallest electrodes with 30-µm droplet spacing on EIS chip with 100-µm electrode-width.

Table 1
Resistances of electrodes, measured electrode widths, ink contact angles and roughness values for different thiol-ene compositions. The electrodes had nominal dimensions of 36 mm x 0.3 mm (l x w). 15-µm droplet spacing was used in this experiment. The width is evaluated from optical micrography. Contact angles marked <5° indicate very low contact angles that were not measurable by goniometry. The roughness values indicate RMS roughness obtained by stylus profilometry.

Composition	5 % Allyl excess	Stoichiometric	5 % Thiol excess	7 % Thiol excess	10 % Thiol excess	30 % Thiol excess
Resistance	60–160 Ω	25–30 Ω	6–40 Ω	1200–1400 Ω	7000–15000 Ω	> 2 M Ω
Width	450 ± 20 µm	320 ± 10 µm	440 ± 40 µm	430 ± 30µm	520 ± 30 µm	570 ± 30 µm
Contact angle	38° ± 6°	13° ± 2°	31° ± 2°	< 5°	< 5°	< 5°
Roughness	2.1 ± 0.3µm	1.6 ± 0.1µm	1.3 ± 0.2µm	1.0 ± 0.1µm	1.5 ± 0.2µm	1.3 ± 0.1µm

the real widths of the electrodes (Fig. 3), the contact angle between the substrate and the ink as well as the roughness of the electrodes were analyzed (Table 1). The analysis shows that the widths of the electrodes were the narrowest, 320 µm, when printed on top of stoichiometric thiol-ene (Fig. 3b). These were also closest to the nominal width of 300 µm. The results also show that the poor conductivity of the higher thiol excess substrates is strongly correlated with the excessive spreading of the ink during printing which is especially pronounced for the 10 % and 30 % thiol excess (Fig. 3e-f) leading to increasingly irregular borders.

There was a clear qualitative difference in the wetting behavior between samples with 5% thiol excess or less and samples with 7% thiol excess or more. Surfaces with 5 % thiol excess or less were wetted by the ink but not completely wetted (the contact angles were between 13°-38°). In stark contrast, surfaces with 7 % or higher thiol excess were completely (or almost completely) wetted by the ink (contact angles were near 0°, which made them too low to be measured). The contact angles are in good agreement with the measured widths of the electrodes with the exception of the stoichiometric substrate, which had low contact angle but still less spreading upon printing compared with substrates of 5% thiol or 5% allyl excess. It is noteworthy that the contact angles were measured in room temperature (vs. printing in 60 °C) and utilizing larger 6 µL droplets than during the printing.

The roughness measurements show some differences between the samples, but these cannot be directly correlated with the differences in resistances. The 7 % thiol excess sample, which is the first sample for which a big jump in the resistivity was observed, is the least rough of all the samples, and it was previously confirmed that the roughness is helpful in obtaining non-cracked and consistently conductive electrodes. However, the samples with 10 % and 30 % thiol excess have very similar roughness compared to the stoichiometric composition. In the SEM images of the electrodes, several crescent shapes (Fig. S2) can be noticed. These are likely polymer islands protruding through the metallic electrodes, which can increase the resistance. However, there were no clear differences in these protrusions between the highly conductive electrodes on 5 % or less thiol excess and the poorly conductive electrodes printed on 7 % or more thiol excess. The differences in conductivity could also be explained by leaching of uncrosslinked monomers from the substrate to the electrode either during printing (at 60 °C) or sintering (at 125 °C).

It has been shown that the adhesion of silver ink into polymers is improved by heating over the glass transition temperature through interfacial fusion [37]. The exact glass transition temperatures of the compositions used in this study were not determined. However, based on values reported in the literature for various compositions of thiol-enes, it seems almost certain that the glass transition temperature for all used compositions were significantly below 125 °C. For a structurally similar polymer with stoichiometric ratio of TMPDE and a tetrathiol (instead of the trithiol used in this study) pentaerythritol tetrakis (2-mercaptoacetate), the Tg was reported to be as low as -35.4 °C [38]. Kwisnek at et al. [39] report glass transition temperatures of various thiol-ene compositions and they fall between −50 °C to 65 °C. Carlborg

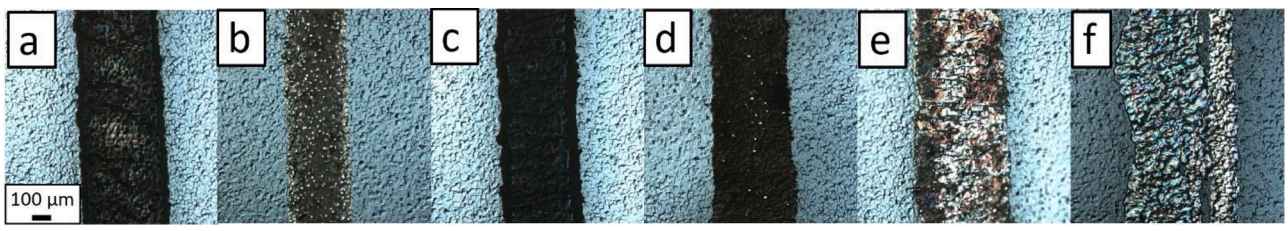

Fig. 3. Optical micrographs of printed electrodes on top of different thiol-ene compositions visualizing the change in the physical appearance of the printed line on top of substrates prepared on substrates with different off-stoichiometric ratios of thiol and allyl monomers. The substrate is (a) 5% allyl excess, (b) stoichiometric, (c) 5% thiol excess, (d) 7% thiol excess, (e) 10 % thiol excess, and (f) 30 % thiol excess. The scalebar in (a) applies to all images. The nominal width of the electrode was 300 µm on all compositions.

et al. [27] reported glass transition temperatures of thiol-enes consisting of a tetrathiol pentaerythritol tetrakis(2-mercaptoacetate) and triallyl-1, 3,5- triazine-2,4,6(1H,3H,5 H)-trione. The glass transition temperatures ranged from approximately 85 °C for the stoichiometric composition to 35 °C for a 100 % thiol excess, which shows that the glass transition temperature tends to be lower for more off-stoichiometric compositions [27]. On this basis, it was concluded that the possible differences in metal-polymer fusion at temperatures above Tg were not likely to explain the observed differences in resistivities since all samples were extremely likely heated above the glass transition temperature and since the samples with the best resistivities were the compositions closer to stoichiometric. However, the metal-polymer fusion can bey an important factor for the overall good adhesion observed in the stretching and bending tests.

3.3. Optimization of printing resolution

The printing resolution was studied with stoichiometric thiol-ene substrates. The resolution on rough substrates was slightly worse than that on smooth substrates due to the ink spreading along the craters of the surface (Fig. 2b and c). However, owing to the poor adhesion and cracking, the electrodes on smooth substrate were not conductive which is why rough substrates were used for the resolution optimization. To achieve conductive electrodes with acceptable repeatability on the rough substrates, at least two adjacent lines of droplets had to be printed to be able to deposit enough of silver nanoparticles, and this limited the minimum line width to ca. 100 µm (with 30-µm droplet spacing) (Fig. 2c).

Single droplet wide electrodes with 30-µm spacing were not conductive because the amount of silver deposited per unit area was too small, and even a small error, e.g. nozzle clogging, could easily make the electrode locally discontinuous. Two droplets wide electrodes tolerated printer errors better than single droplet wide electrodes, although the single droplet wide were printable too when the droplet spacing was lowered to 15-µm. With both droplet spacings, a single layer of ink was enough and therefore multiple layers of ink were not tested.

The minimum achieved electrode gap was limited by the droplet spacing and droplet spreading. Here, the droplet spacing used was 30 µm and the diameter of deposited droplets on the thiol-ene substrate was 75 µm. These limited the possible gaps between two electrodes to start from 20 µm and increasing with 30-µm steps. Electrode merging occurred often with gaps of 20 µm and 50 µm, and thus the minimum gap between two fully separated lines that could be reliably fabricated was 80 µm.

3.4. Electrode bend and stretch tests

Electrode stretching and bending were tested with electrodes printed on 0.5 mm and 2 mm thick rough stoichiometric thiol-ene substrates. The dimensions of the electrodes in the strain tests were 3.6 mm x 0.3 mm (L x W) with 2 mm x 2 mm contact pads at both ends.

The electrodes were characterized optically and electrically before and after the experiments. Table 2 summarizes the strain experiments. The bending was performed in two directions to expose the wires to compressive and tensile forces. The maximum elastic strain for both substrate thicknesses was the same, approximately 5 %. When the strain exceeded 5 %, the thiol-ene itself fractured but there was no metal adhesion loss.

The 0.5 mm thick substrate tolerated bending (Fig. 4) down to radius of curvature of approximately 2.5 mm without any loss of conductivity and the electrodes were intact and conductive even when bent to a 1 mm radius of curvature albeit small cracks were observed. The 2 mm substrate tolerated bending to approximately 20 mm radius of curvature without loss of conductivity. Attempts to bend the 2 mm substrates on radius of curvature <20 mm lead to the thiol-ene layer fracturing in half before any cracking of the electrodes themselves. Electrode adhesion loss was not observed in the bending experiments.

3.5. Electrochemical impedance spectroscopy

Electrochemical impedance spectroscopy (EIS) is a method utilizing a pair of electrodes for *in situ* monitoring of the material-cell interactions on BioMEMS devices. Changes in cell layer coverage on electrodes alter the electrode-solution interface, which in turn affects the system's impedance [40]. In addition, alterations in cell morphology, cell-cell, and cell-substrate interactions provoke changes in signal. The most common application of EIS is to study barrier function of endothelial cells, but in general, cell proliferation, changes in layer architecture and cell morphology of any adherent cell type are detectable by EIS. In

Fig. 4. Flexible thiol-ene electrodes. Thiol-ene (thickness 0.5 mm) is bent over a radius of 2 mm resulting in negligible change in resistances of the electrodes.

Table 2
Bend and stretch experiments for inkjet-printed straight-line electrodes on stoichiometric thiol-ene. In stress column, r indicates the radius of bending. Resistances are averages over five electrodes across chip. N/A means that the thiol-ene fractured in two pieces so the electrode resistance could not be measured.

Substrate thickness	Type of stress	No. of cycles	Resistance, Ω		Optical inspection	
			Before	After	Before	After
0.5 mm	Bend, r = 2.5 mm	10	70–100	70–100	Continuous	Continuous
	Bend, r = 1.0 mm	5	70–100	130–150	Continuous	Small cracks
	Bend, r < 1.0 mm	1	70–100	N/A	Continuous	Broken
	Stretch, 5 %	10	70–100	100–120	Continuous	Small cracks
2 mm	Bend, r = 20 mm	10	60–150	60–150	Continuous	Continuous
	Bend, r < 20 mm	1	60–150	N/A	Continuous	Broken
	Stretch, 5 %	10	60–150	100–150	Continuous	Small cracks

combination with other fluorescent end-point detection methodologies, non-invasive EIS monitoring of cells can be utilized to produce complementary information *in situ* regarding e.g. drug effects [41] or disruption of cell-cell junctions and cell-substrate interactions [42] over time. In addition, material-induced toxicity (e.g., due to leaching monomers or ink-derived contaminants) is shown in the EIS signal, so it serves as a method to evaluate materials' cell-compatibility.

In this study, stoichiometric thiol-ene was chosen for the fabrication of the EIS chips for two reasons: 1) the low resistance of silver on this particular composition, and 2) to reduce the amount of uncrosslinked monomers that might leak into the cell culture and impair cell proliferation [43]. The EIS electrodes were printed with a 30-μm droplet spacing and at least 110-μm gap between the electrodes and were 100−750 μm wide (depending of the sample) with interdigitated two-, three- or five-finger patterns to maximize the sensing area (Fig. 5a-b). The EIS electrodes had contact pads of 2 mm x 3 mm, and the tracers leading to the pads were 300 μm wide (Fig. 5b). In addition, two electrode widths for the five-finger pattern were tested (100 μm and 200 μm). Fig. 5c and d show electrode printing design and actual silver print, respectively. As expected, increase in the number of fingers increased the difference between maximum and minimum signal intensities within the range of frequencies (between 5–100 000 Hz) tested. Thus, the possibility to customize the electrode array design on demand, by simply printing a new pattern, provided a convenient means for optimization of the EIS signal (Fig. 6a).

The five-fingered pattern with 100-μm wide electrodes was chosen for further cell culturing assays. The adherent 3T3 cells were grown directly onto the electrodes and were shown to alter the impedance at the electrode-solution interface (Fig. 6b). The use of interdigitated working and counter electrodes of the same size aims at measuring changes in cell layer coverage of a large area [40]. The maximum difference in signal was detected at 8 kHz (Fig. 6b). To confirm that the changes in impedance signal during the 36-h growth period were resulting from increased cell monolayer integrity, the viable and dead cells were stained with fluorescent markers (Fig. 7), which evidenced good cell coverage and negligible number of dead cells both on thiol-enes (Fig. 7a-d) and on top of the electrodes (Fig. 7e-h). Based on the EIS experiments, it could be concluded that the printed electrodes clearly withstood the conditions in the cell culture medium at 37 °C for at least 36 h. In addition, the cells remained viable over the same period of time when in direct contact with the silver electrodes and the stoichiometric thiol-ene substrate, suggesting that there were no issues with chemical contaminants leaching from the bulk of the printed patterns.

4. Conclusions

Inkjet printing of silver nanoparticle ink directly on thiol-ene polymers provided conductive and flexible electrodes feasible for, e.g., wearable electronics. A key finding was that the printing quality was vastly improved by utilizing rough surfaces. In this study, the micron level roughness, that was found critical to ensuring good adhesion of the ink, was obtained simply by replicating the substrate from an unpolished silicon wafer. With optimized printing parameters, inkjet printing of silver on top of rough substrates yielded 100 μm wide electrodes and 80 μm gaps as the resolution threshold. The obtained resistivity depended on the composition of the thiol-enes; good resistivity down to 30 μΩcm could be achieved with compositions close to stoichiometric. The electrodes were flexible and their conductivity remained unchanged after repeated bending although the tolerance to linear strain was limited to 5 % due to the mechanical properties of thiol-ene itself. The biocompatibility of the printed electrodes was confirmed by impedance-based monitoring of cells cultured on top of the printing media for 36 h. The electrodes also survived well in stressed conditions (37 °C, wet) typical for cell cultures without any protective coating. Besides wearable sensors, the developed metallization scheme could greatly benefit various microfluidic devices necessitating electrical or electrochemical

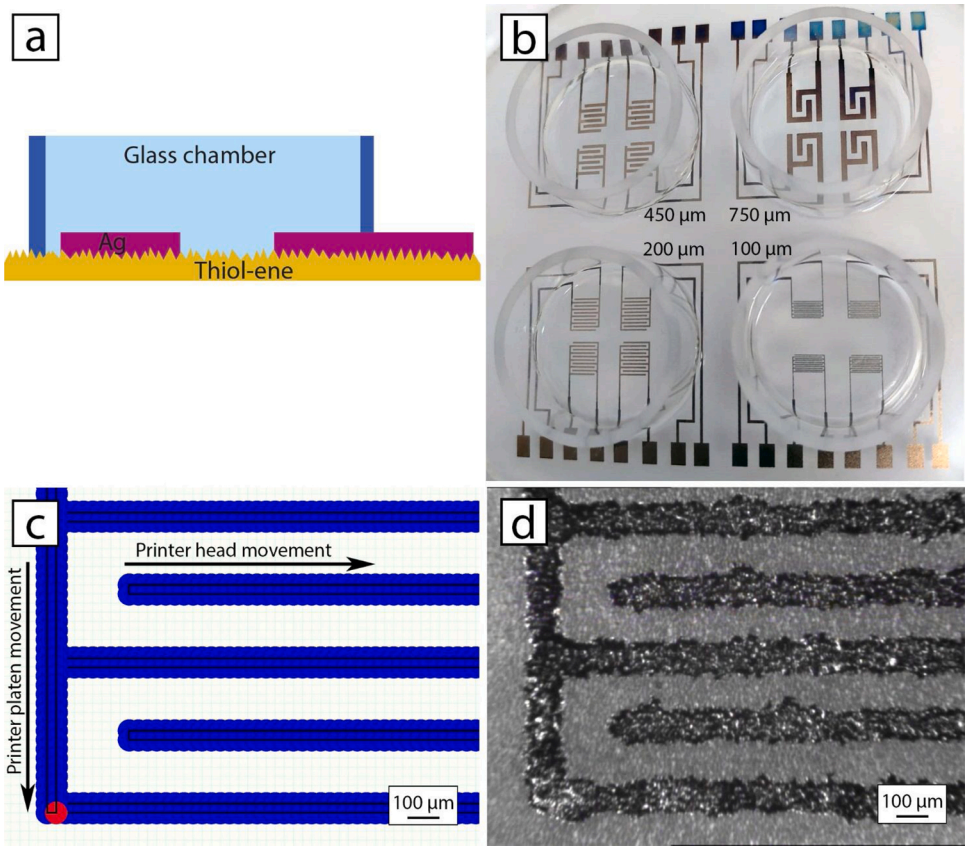

Fig. 5. Printed electrodes for EIS. (a) Schematic cross-section of the EIS chip with glued glass-chamber enclosing sintered Ag-electrodes on top of rough thiol-ene. (b) EIS chip designs with the glued glass chambers. Dimensions in the middle indicate electrode width; (c) layout of the 100 μm design, where black lines show the programmed places for droplets, and blue circles (gray in print version) illustrate final droplet spreading on the substrate. One droplet is highlighted at the bottom left corner; and (d) microscope image of the 100 μm design.

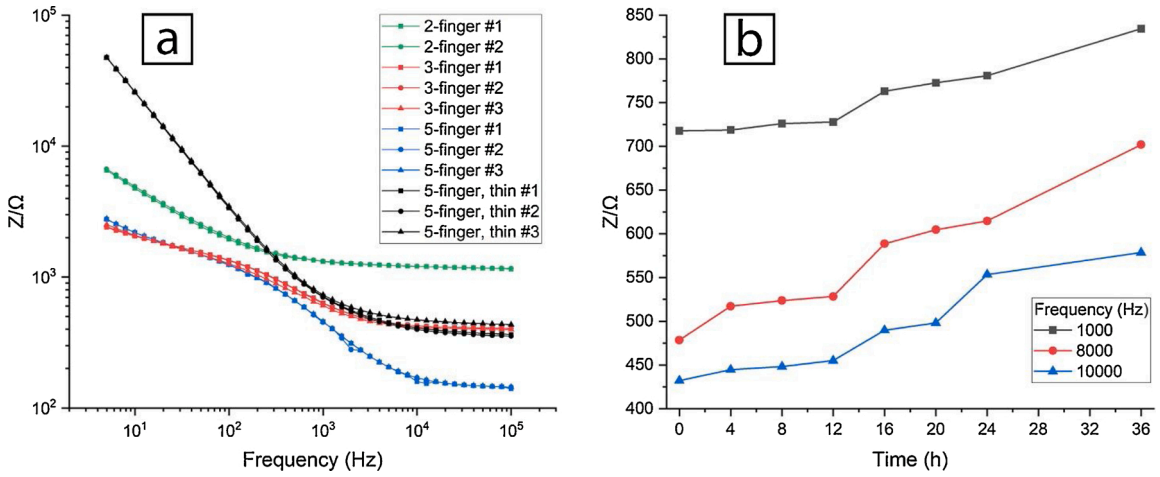

Fig. 6. Impedance spectroscopy results: (a) the effect of electrode design on impedance spectra after loading the wells with cell culture medium and cells (0 h). Total of four differently interdigitated designs were studied to optimize the spectral profiles, including 2-, 3- and 5-finger designs. Electrode width was 220 μm except for "thin" which was 100 μm. (b) The evolution of the impedance signal during a 36-h-long cell culturing period at three different frequencies. The electrode design used is the 5-finger design with 100 μm wide electrodes.

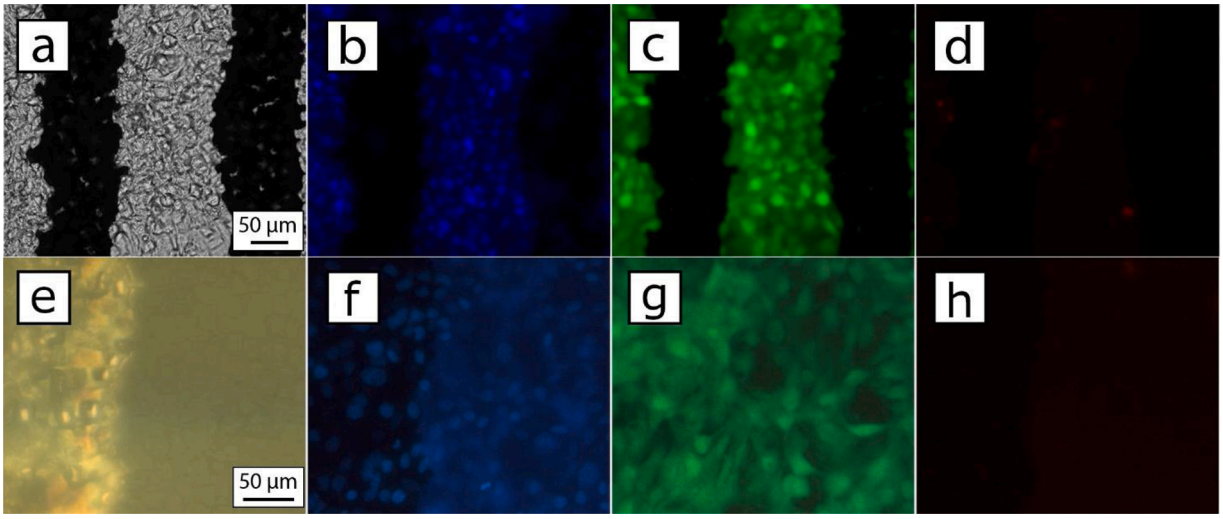

Fig. 7. Micrographs of 3T3 cells grown (36 h) on silver electrodes printed on stoichiometric thiol-ene. (a)-(d) show the same spot and the same scale bar applies to all of them. (e)-(h) show the same spot with the same scale bar applying to all of them. The micrographs (a)-(d) are taken with an inverted epifluorescence microscope and thus the electrodes block the light path and appear as black lines. The micrographs (e)-(h) are taken with an upright epifluorescence microscope and thus show the cells grown on the electrodes. (a),(e) Bright-field micrographs. (b)-(d), (f)-(h) Fluoresence micrographs of cells stained with (b),(f) Hoechst 33,342 (all nuclei); (c), (g) Calcein AM (viable cells); and (d),(h) propidium iodide (dead cells).

readout, as the protocol omits the need for vacuum deposition, lithography and etching steps.

CRediT authorship contribution statement

Eero Kuusisto: Investigation, Writing - original draft, Writing - review & editing. **Joonas J. Heikkinen:** Investigation, Writing - original draft. **Päivi Järvinen:** Investigation, Writing - review & editing. **Tiina Sikanen:** Conceptualization, Writing - review & editing, Resources. **Sami Franssila:** Conceptualization, Writing - review & editing, Supervision, Funding acquisition. **Ville Jokinen:** Conceptualization, Investigation, Writing - review & editing, Supervision.

Declaration of Competing Interest

The authors declare no competing financial interests.

Acknowledgements

Funding from Academy of Finland (projects #297360, 308911 and 309608) are acknowledged. The work utilized the cleanroom facilities of OtaNano research infrastructure of Micronova Centre for Micro and Nanotechnology. E. Kuusisto and JJ. Heikkinen contributed equally to this work.

Appendix A. Supplementary data

Supplementary material related to this article can be found, in the online version, at doi:https://doi.org/10.1016/j.snb.2021.129727.

References

[1] M. Gao, L. Li, Y. Song, Inkjet printing wearable electronic devices, J. Mater. Chem. C. 5 (2017) 2971–2993, https://doi.org/10.1039/C7TC00038C.

[2] K. Yamada, T.G. Henares, K. Suzuki, D. Citterio, Paper-based inkjet-printed microfluidic analytical devices, Angew. Chem. Int. Ed. 54 (2015) 5294–5310, https://doi.org/10.1002/anie.201411508.
[3] H. Sirringhaus, T. Kawase, R.H. Friend, T. Shimoda, M. Inbasekaran, W. Wu, E. P. Woo, High-resolution inkjet printing of all-polymer, Transistor Circuits 290 (2000) 5.
[4] Y. Sun, Y. Zhang, Q. Liang, Y. Zhang, H. Chi, Y. Shi, D. Fang, Solvent inkjet printing process for the fabrication of polymer solar cells, RSC Adv. 3 (2013) 11925, https://doi.org/10.1039/c3ra22659j.
[5] A. Määttänen, U. Vanamo, P. Ihalainen, P. Pulkkinen, H. Tenhu, J. Bobacka, J. Peltonen, A low-cost paper-based inkjet-printed platform for electrochemical analyses, Sens. Actuators B Chem. 177 (2013) 153–162, https://doi.org/10.1016/j.snb.2012.10.113.
[6] R.E. Saunders, B. Derby, Inkjet printing biomaterials for tissue engineering: bioprinting, Int. Mater. Rev. 59 (2010) 430–448, https://doi.org/10.1179/1743280414Y.0000000040.
[7] C. Gaspar, T. Sikanen, S. Franssila, V. Jokinen, Inkjet printed silver electrodes on macroporous paper for a paper-based isoelectric focusing device, Biomicrofluidics. 10 (2016), 064120, https://doi.org/10.1063/1.4973246.
[8] S. Jang, Y. Seo, J. Choi, T. Kim, J. Cho, S. Kim, D. Kim, Sintering of inkjet printed copper nanoparticles for flexible electronics, Scr. Mater. 62 (2010) 258–261, https://doi.org/10.1016/j.scriptamat.2009.11.011.
[9] Y. Gao, W. Shi, W. Wang, Y. Leng, Y. Zhao, Inkjet printing patterns of highly conductive pristine graphene on flexible substrates, Ind. Eng. Chem. Res. 53 (2014) 16777–16784, https://doi.org/10.1021/ie502675z.
[10] S. Kholghi Eshkalak, A. Chinnappan, W.A.D.M. Jayathilaka, M. Khatibzadeh, E. Kowsari, S. Ramakrishna, A review on inkjet printing of CNT composites for smart applications, Appl. Mater. Today 9 (2017) 372–386, https://doi.org/10.1016/j.apmt.2017.09.003.
[11] J.T. Delaney, P.J. Smith, U.S. Schubert, Inkjet printing of proteins, Soft Matter 5 (2009) 4866, https://doi.org/10.1039/b909878j.
[12] P.W. Cooley, D.B. Wallace, B.V. Antohe, in: C.H. Mastrangelo, H. Becker (Eds.), Applications of Ink-Jet Printing Technology to BioMEMS and Microfluidic Systems, 2001, pp. 177–188, https://doi.org/10.1117/12.443057. San Francisco, CA.
[13] S.H. Ko, H. Pan, C.P. Grigoropoulos, C.K. Luscombe, J.M.J. Fréchet, D. Poulikakos, All-inkjet-printed flexible electronics fabrication on a polymer substrate by low-temperature high-resolution selective laser sintering of metal nanoparticles, Nanotechnology. 18 (2007), 345202, https://doi.org/10.1088/0957-4484/18/34/345202.
[14] A. Kamyshny, Metal-based inkjet inks for printed electronics, TOAPJ. 4 (2011) 19–36, https://doi.org/10.2174/1874183501104010019.
[15] A. Kamyshny, S. Magdassi, Conductive nanomaterials for printed electronics, Small 10 (2014) 3515–3535, https://doi.org/10.1002/smll.201303000.
[16] T.H.J. van Osch, J. Perelaer, A.W.M. de Laat, U.S. Schubert, Inkjet printing of narrow conductive tracks on untreated polymeric substrates, Adv. Mater 20 (2008) 343–345, https://doi.org/10.1002/adma.200701876.
[17] V. Subramanian, J.M.J. Frechet, P.C. Chang, D.C. Huang, J.B. Lee, S.E. Molesa, A. R. Murphy, D.R. Redinger, S.K. Volkman, Progress toward development of all-printed RFID tags: materials, processes, and devices, Proc. IEEE. 93 (2005) 1330–1338, https://doi.org/10.1109/JPROC.2005.850305.
[18] N.C. Raut, K. Al-Shamery, Inkjet printing metals on flexible materials for plastic and paper electronics, J. Mater. Chem. C. 6 (2018) 1618–1641, https://doi.org/10.1039/C7TC04804A.
[19] T. Öhlund, J. Örtegren, S. Forsberg, H.-E. Nilsson, Paper surfaces for metal nanoparticle inkjet printing, Appl. Surf. Sci. 259 (2012) 731–739, https://doi.org/10.1016/j.apsusc.2012.07.112.
[20] J.C. McDonald, G.M. Whitesides, Poly(dimethylsiloxane) as a material for fabricating microfluidic devices, Acc. Chem. Res. 35 (2002) 491–499, https://doi.org/10.1021/ar010110q.
[21] A. Mata, A.J. Fleischman, S. Roy, Characterization of polydimethylsiloxane (PDMS) properties for biomedical Micro/Nanosystems, Biomed. Microdevices 7 (2005) 281–293, https://doi.org/10.1007/s10544-005-6070-2.
[22] J. Wu, R. Wang, H. Yu, G. Li, K. Xu, N.C. Tien, R.C. Roberts, D. Li, Inkjet-printed microelectrodes on PDMS as biosensors for functionalized microfluidic systems, Lab Chip 15 (2015) 690–695, https://doi.org/10.1039/C4LC01121J.
[23] K. Sondhi, S. Hwangbo, Y.-K. Yoon, T. Nishida, Z.H. Fan, Airbrushing and surface modification for fabricating flexible electronics on polydimethylsiloxane, J. Micromech. Microeng. 28 (2018), 125014, https://doi.org/10.1088/1361-6439/aae9d6.
[24] S. Chung, J. Lee, H. Song, S. Kim, J. Jeong, Y. Hong, Inkjet-printed stretchable silver electrode on wave structured elastomeric substrate, Appl. Phys. Lett. 98 (2011), 153110, https://doi.org/10.1063/1.3578398.
[25] M. Kanungo, S. Mettu, K.-Y. Law, S. Daniel, Effect of roughness geometry on wetting and dewetting of rough PDMS surfaces, Langmuir. 30 (2014) 7358–7368, https://doi.org/10.1021/la404343n.
[26] C.E. Hoyle, C.N. Bowman, Thiol-ene click chemistry, Angew. Chemie Int. Ed. 49 (2010) 1540–1573, https://doi.org/10.1002/anie.200903924.
[27] C.F. Carlborg, T. Haraldsson, K. Öberg, M. Malkoch, W. van der Wijngaart, Beyond PDMS: off-stoichiometry thiol–ene (OSTE) based soft lithography for rapid prototyping of microfluidic devices, Lab Chip 11 (2011) 3136, https://doi.org/10.1039/c1lc20388f.
[28] T.M. Sikanen, J.P. Lafleur, M.-E. Moilanen, G. Zhuang, T.G. Jensen, J.P. Kutter, Fabrication and bonding of thiol-ene-based microfluidic devices, J. Micromech. Microeng. 23 (2013), 037002, https://doi.org/10.1088/0960-1317/23/3/037002.
[29] S. Mongkhontreerat, K. Öberg, L. Erixon, P. Löwenhielm, A. Hult, M. Malkoch, UV initiated thiol–ene chemistry: a facile and modular synthetic methodology for the construction of functional 3D networks with tunable properties, J. Mater. Chem. A. 1 (2013), 13732, https://doi.org/10.1039/c3ta12963b.
[30] D. Sticker, M. Rothbauer, S. Lechner, M.-T. Hehenberger, P. Ertl, Multi-layered, membrane-integrated microfluidics based on replica molding of a thiol–ene epoxy thermoset for organ-on-a-chip applications, Lab Chip 15 (2015) 4542–4554, https://doi.org/10.1039/C5LC01028D.
[31] S.M. Tähkä, A. Bonabi, M.-E. Nordberg, M. Kanerva, Ville P. Jokinen, T.M. Sikanen, Thiol-ene microfluidic devices for microchip electrophoresis: Effects of curing conditions and monomer composition on surface properties, J. Chromatogr. A 1426 (2015) 233–240, https://doi.org/10.1016/j.chroma.2015.11.072.
[32] S. Tähkä, J. Sarfraz, L. Urvas, R. Provenzani, S.K. Wiedmer, J. Peltonen, V. Jokinen, T. Sikanen, Immobilization of proteolytic enzymes on replica-molded thiol-ene micropillar reactors via thiol-gold interaction, Anal. Bioanal. Chem. 411 (2019) 2339–2349, https://doi.org/10.1007/s00216-019-01674-9.
[33] A. Ulman, J.F. Kang, Y. Shnidman, S. Liao, R. Jordan, G.-Y. Choi, J. Zaccaro, A. S. Myerson, M. Rafailovich, J. Sokolov, C. Fleischer, Self-assembled monolayers of rigid thiols, Rev. Mol. Biotechnol. 74 (2000) 175–188, https://doi.org/10.1016/S1389-0352(00)00013-1.
[34] J. Bae, Y. Yang, Thiol-ene/hyperbranched polymer hybrid thin films: cure behavior and gas barrier properties, J. Non. Solids 357 (2011) 3103–3107, https://doi.org/10.1016/j.jnoncrysol.2011.04.019.
[35] A. Müller, M.C. Wapler, U. Wallrabe, A quick and accurate method to determine the Poisson's ratio and the coefficient of thermal expansion of PDMS, Soft Matter 15 (2019) 779–784, https://doi.org/10.1039/C8SM02105H.
[36] J.-T. Wu, S.L.-C. Hsu, M.-H. Tsai, W.-S. Hwang, Direct inkjet printing of silver Nitrate/Poly(*N* -vinyl-2-pyrrolidone) inks to fabricate silver conductive lines, J. Phys. Chem. C. 114 (2010) 4659–4662, https://doi.org/10.1021/jp100326k.
[37] T. Sekine, K. Fukuda, D. Kumaki, S. Tokito, Enhanced adhesion mechanisms between printed nano-silver electrodes and underlying polymer layers, Nanotechnology 26 (2015), 321001.
[38] P. Shen, S.Z. Moghaddam, Q. Huang, A.E. Daugaard, S. Zhang, P. Szabo, Hard-soft thiol-ene materials without interfacial weakness, Mater. Today Commun. 21 (2019), 100657, https://doi.org/10.1016/j.mtcomm.2019.100657.
[39] L. Kwisnek, S. Nazarenko, C.E. Hoyle, Oxygen transport properties of thiol−Ene networks, Macromolecules 42 (2009) 7031–7041, https://doi.org/10.1021/ma901117s.
[40] J.A. Stolwijk, K. Matrougui, C.W. Renken, M. Trebak, Impedance analysis of GPCR-mediated changes in endothelial barrier function: overview and fundamental considerations for stable and reproducible measurements, Pflugers Arch Eur. J. Physiol. 467 (2015) 2193–2218, https://doi.org/10.1007/s00424-014-1674-0.
[41] M. Parviz, K. Gaus, J.J. Gooding, Simultaneous impedance spectroscopy and fluorescence microscopy for the real-time monitoring of the response of cells to drugs, Chem. Sci. 8 (2017) 1831–1840, https://doi.org/10.1039/C6SC05159F.
[42] B.R. Brückner, H. Nöding, M. Skamrahl, A. Janshoff, Mechanical and morphological response of confluent epithelial cell layers to reinforcement and dissolution of the F-actin cytoskeleton, Prog. Biophys. Mol. Biol. 144 (2019) 77–90, https://doi.org/10.1016/j.pbiomolbio.2018.08.010.
[43] K. Piironen, P. Järvinen, I. Kiiski, T. Sikanen, Understanding cell proliferation and material induced cell death on microfluidic devices made of off stoichiometric thiol-enes, Proceedings of MicroTAS (2019).

Eero Kuusisto is a M.Sc. student at Aalto University, School of Chemical Engineering, Functional Materials masters program. His research interests include microfabrication and novel materials.

Joonas Heikkinen is a Ph.D. student at Aalto University, School of Chemical Engineering. His Ph.D. work focuses on microfabrication of carbon materials and their use in electrical and electrochemical sensing.

Tiina Sikanen is a principal investigator at the Faculty of Pharmacy, University of Helsinki (UH), Finland. She obtained her PhD in pharmaceutical chemistry (UH) in 2007. Her research focuses on bioinspired microfluidics and bridges drug metabolism, mass spectrometry, and materials sciences, including polymer microfabrication and biofunctionalization.

Päivi Järvinen (PhD pharm.) is a University Researcher at the Faculty of Pharmacy, University of Helsinki (UH), Finland. Her research focuses on developing cell-based assays for microfluidic settings to study drug effects and metabolism.

Sami Franssila is a professor of materials science at Aalto University, Helsinki, Finland. He received the B.Sc. and M.Sc. degrees in physics from the University of Helsinki, Helsinki, Finland, and the Ph.D. degree in 1995 from Helsinki University of Technology, with a thesis on plasma etching. He worked at VTT and IMEC on CMOS and MEMS technologies before joining Aalto University in 1998. His research since then has been mostly on micro and nanofabrication for fluidic, bio and thermal devices. He has authored or coauthored over 160 peer-reviewed journal articles and the textbook *Introduction to Microfabrication* (John Wiley, 2010).

Ville Jokinen is a University Lecturer at Aalto University, School of Chemical Engineering, Finland. He obtained his M.Sc. in 2007 in Engineering Physics from Aalto University and his Ph.D. in 2011 from University of Helsinki, Faculty of Medicine, Finland. His main research interests are microfabrication methods, microfluidics, wetting and surfaces and especially the applications of these in the biomedical field.